



A Reconciled Estimate of Ice-Sheet Mass Balance

Andrew Shepherd *et al.*

Science **338**, 1183 (2012);

DOI: 10.1126/science.1228102

This copy is for your personal, non-commercial use only.

If you wish to distribute this article to others, you can order high-quality copies for your colleagues, clients, or customers by [clicking here](#).

Permission to republish or repurpose articles or portions of articles can be obtained by following the guidelines [here](#).

The following resources related to this article are available online at www.sciencemag.org (this information is current as of November 29, 2012):

Updated information and services, including high-resolution figures, can be found in the online version of this article at:

<http://www.sciencemag.org/content/338/6111/1183.full.html>

Supporting Online Material can be found at:

<http://www.sciencemag.org/content/suppl/2012/11/28/338.6111.1183.DC1.html>

A list of selected additional articles on the Science Web sites **related to this article** can be found at:

<http://www.sciencemag.org/content/338/6111/1183.full.html#related>

This article **cites 156 articles**, 29 of which can be accessed free:

<http://www.sciencemag.org/content/338/6111/1183.full.html#ref-list-1>

This article has been **cited by** 1 articles hosted by HighWire Press; see:

<http://www.sciencemag.org/content/338/6111/1183.full.html#related-urls>

This article appears in the following **subject collections**:

Atmospheric Science

<http://www.sciencemag.org/cgi/collection/atmos>

the assembly. However, in practice, low yields were already observed for larger designs (up to 24,576 nucleotides attempted thus far). Solving this challenge may require improvements in structure and sequence design, enzymatic synthesis for higher-quality strands, optimized thermal or isothermal (44) annealing conditions, and a detailed understanding and perhaps explicit engineering of the kinetic assembly pathways (8, 14, 44) of DNA brick structures.

The DNA brick structure, with its modular architecture, sophisticated geometry control, and synthetic nature, will further expand the range of applications and challenges that nucleic acid nanotechnology has already started to address—for example, to arrange technologically relevant guest molecules into functional devices (6, 25, 32–34), to serve as programmable molecular probes and instruments for biological studies (33, 34, 36), to render spatial control for biosynthesis of useful products (25), to function as smart drug delivery particles (37), and to enable high-throughput nanofabrication of complex inorganic materials for electronics or photonics applications (6, 32). The modularity of the brick structure may facilitate rapid prototyping of diverse functional nanodevices. Its sophisticated and refined geometrical control may enable applications that require high-precision arrangements of guest molecules. Because the brick structure is composed entirely of short synthetic strands (no biologically derived scaffold), it is conceivable to make bricks by using synthetic informational polymers other than the natural form of DNA. Such polymers may include L-DNA (26), DNA with chemically modified backbones or artificial bases, or chemically synthesized or in vitro (or even in vivo) transcribed RNA. This material diversity may potentially produce nanostructures with not only prescribed shapes but also designer chemical (or biochemical) properties (such as nuclease resistance or reduced immunogenicity) that would be useful for diverse applications requiring the structure to function robustly in complex environments, such as in living cells or organisms.

References and Notes

- N. C. Seeman, *J. Theor. Biol.* **99**, 237 (1982).
- J. H. Chen, N. C. Seeman, *Nature* **350**, 631 (1991).
- T. J. Fu, N. C. Seeman, *Biochemistry* **32**, 3211 (1993).
- E. Winfree, F. Liu, L. A. Wenzler, N. C. Seeman, *Nature* **394**, 539 (1998).
- B. Yurke, A. J. Turberfield, A. P. Mills Jr., F. C. Simmel, J. L. Neumann, *Nature* **406**, 605 (2000).
- H. Yan, S. H. Park, G. Finkelstein, J. H. Reif, T. H. LaBean, *Science* **301**, 1882 (2003).
- W. B. Sherman, N. C. Seeman, *Nano Lett.* **4**, 1203 (2004).
- P. W. K. Rothemund, N. Papadakis, E. Winfree, *PLoS Biol.* **2**, e424 (2004).
- A. Chworos et al., *Science* **306**, 2068 (2004).
- S. H. Park et al., *Angew. Chem. Int. Ed.* **45**, 735 (2006).
- P. W. K. Rothemund, *Nature* **440**, 297 (2006).
- G. Seelig, D. Soloveichik, D. Y. Zhang, E. Winfree, *Science* **314**, 1585 (2006).
- Y. He et al., *Nature* **452**, 198 (2008).
- P. Yin, H. M. T. Choi, C. R. Calvert, N. A. Pierce, *Nature* **451**, 318 (2008).
- P. Yin et al., *Science* **321**, 824 (2008).
- E. S. Andersen et al., *Nature* **459**, 73 (2009).
- Y. Ke et al., *Nano Lett.* **9**, 2445 (2009).
- S. M. Douglas et al., *Nature* **459**, 414 (2009).
- H. Dietz, S. M. Douglas, W. M. Shih, *Science* **325**, 725 (2009).
- J. Zheng et al., *Nature* **461**, 74 (2009).
- T. Omabegho, R. Sha, N. C. Seeman, *Science* **324**, 67 (2009).
- I. Severcan et al., *Nat. Chem.* **2**, 772 (2010).
- D. Han et al., *Science* **332**, 342 (2011).
- L. Qian, E. Winfree, *Science* **332**, 1196 (2011).
- C. J. Delebecque, A. B. Lindner, P. A. Silver, F. A. Aldaye, *Science* **333**, 470 (2011).
- B. Wei, M. Dai, P. Yin, *Nature* **485**, 623 (2012).
- C. Lin, Y. Liu, S. Rinker, H. Yan, *ChemPhysChem* **7**, 1641 (2006).
- N. B. Leontis, A. Lescoute, E. Westhof, *Curr. Opin. Struct. Biol.* **16**, 279 (2006).
- W. M. Shih, C. Lin, *Curr. Opin. Struct. Biol.* **20**, 276 (2010).
- N. C. Seeman, *Annu. Rev. Biochem.* **79**, 65 (2010).
- D. Y. Zhang, G. Seelig, *Nat. Chem.* **3**, 103 (2011).
- A. Kuzyk et al., *Nature* **483**, 311 (2012).
- H. M. T. Choi et al., *Nat. Biotechnol.* **28**, 1208 (2010).
- C. Lin et al., *Nat. Chem.* **4**, 832 (2012).
- M. J. Berardi, W. M. Shih, S. C. Harrison, J. J. Chou, *Nature* **476**, 109 (2011).
- N. D. Derr et al., *Science* **338**, 662 (2012).
- S. M. Douglas, I. Bachelet, G. M. Church, *Science* **335**, 831 (2012).
- P. W. K. Rothemund, E. S. Andersen, *Nature* **485**, 584 (2012).
- Materials and methods, supplementary figures and texts, and DNA sequences are available as supplementary materials on Science Online.
- S. M. Douglas et al., *Nucleic Acids Res.* **37**, 5001 (2009).
- Y. Ke et al., *J. Am. Chem. Soc.* **131**, 15903 (2009).
- C. E. Castro et al., *Nat. Methods* **8**, 221 (2011).
- Y. Ke, N. V. Voigt, K. V. Gothelf, W. M. Shih, *J. Am. Chem. Soc.* **134**, 1770 (2012).
- R. Schulman, B. Yurke, E. Winfree, *Proc. Natl. Acad. Sci. U.S.A.* **109**, 6405 (2012).

Acknowledgments: The authors thank M. Dai for technical assistance; E. Winfree, B. Wei, and S. Woo for discussions; and D. Pastuszak for assistance in draft preparation. This work is supported by an Office of Naval Research (ONR) Young Investigator Program award N000141110914, an ONR grant N000141010827, an Army Research Office grant W911NF1210238, an NSF CAREER award CCF1054898, an NIH Director's New Innovator award 1DP2OD007292, and a Wyss Institute Faculty Startup Fund to P.Y., and by a Wyss Institute Faculty Grant, ONR grants N00014091118 and N000141010241, and an NIH Director's New Innovator award 1DP2OD004641 to W.M.S.. L.L.O. is supported by an NSF graduate research fellowship. Y.K. conceived the project, designed and performed the experiments, analyzed the data, and wrote the paper; L.L.O. designed and performed the experiments, analyzed the data, and wrote the paper; W.M.S. conceived the project, discussed the results, and wrote the paper; P.Y. conceived, designed, and supervised the study, interpreted the data, and wrote the paper. The DNA sequences for the nanostructures can be found in the supplementary materials. A provisional patent has been filed based on this work.

Supplementary Materials

www.sciencemag.org/cgi/content/full/338/6111/1177/DC1
Materials and Methods
Supplementary Text
Figs. S1 to S66
Tables S1 to S20

11 July 2012; accepted 16 October 2012
10.1126/science.1227268

A Reconciled Estimate of Ice-Sheet Mass Balance

Andrew Shepherd,^{1*} Erik R. Ivins,^{2*} Geruo A.,³ Valentina R. Barletta,⁴ Mike J. Bentley,⁵ Srinivas Bettadpur,⁶ Kate H. Briggs,¹ David H. Bromwich,⁷ René Forsberg,⁴ Natalia Galin,⁸ Martin Horwath,⁹ Stan Jacobs,¹⁰ Ian Joughin,¹¹ Matt A. King,^{12,27} Jan T. M. Lenaerts,¹³ Jilu Li,¹⁴ Stefan R. M. Ligtenberg,¹³ Adrian Luckman,¹⁵ Scott B. Luthcke,¹⁶ Malcolm McMillan,¹ Rakia Meister,⁸ Glenn Milne,¹⁷ Jeremie Mouginot,¹⁸ Alan Muir,⁸ Julien P. Nicolas,⁷ John Paden,¹⁴ Antony J. Payne,¹⁹ Hamish Pritchard,²⁰ Eric Rignot,^{18,2} Helmut Rott,²¹ Louise Sandberg Sørensen,⁴ Ted A. Scambos,²² Bernd Scheuchl,¹⁸ Ernst J. O. Schrama,²³ Ben Smith,¹¹ Aud V. Sundal,¹ Jan H. van Angelen,¹³ Willem J. van de Berg,¹³ Michiel R. van den Broeke,¹³ David G. Vaughan,²⁰ Isabella Velicogna,^{18,2} John Wahr,³ Pippa L. Whitehouse,⁵ Duncan J. Wingham,⁸ Donghui Yi,²⁴ Duncan Young,²⁵ H. Jay Zwally²⁶

We combined an ensemble of satellite altimetry, interferometry, and gravimetry data sets using common geographical regions, time intervals, and models of surface mass balance and glacial isostatic adjustment to estimate the mass balance of Earth's polar ice sheets. We find that there is good agreement between different satellite methods—especially in Greenland and West Antarctica—and that combining satellite data sets leads to greater certainty. Between 1992 and 2011, the ice sheets of Greenland, East Antarctica, West Antarctica, and the Antarctic Peninsula changed in mass by -142 ± 49 , $+14 \pm 43$, -65 ± 26 , and -20 ± 14 gigatonnes year⁻¹, respectively. Since 1992, the polar ice sheets have contributed, on average, 0.59 ± 0.20 millimeter year⁻¹ to the rate of global sea-level rise.

Fluctuations in the mass of the polar ice sheets are of considerable societal importance, because they affect global sea levels (1, 2) and oceanic conditions. They occur as

a consequence of their internal dynamics and changes in atmospheric and oceanic conditions (3–5). Analysis of the geological record suggests that past climatic changes have precipitated

sustained ice-sheet contributions, in excess of 10 mm year⁻¹ over millennial time periods (6), and the prospect of such changes in the future are of greatest concern. Even the modest rises in ocean temperature that are predicted over the coming century (7) could trigger substantial ice-sheet mass loss through enhanced melting of ice shelves (8–10) and outlet glaciers (11, 12). However, these processes were not incorporated into the ice-sheet models that informed the current global climate projections (13). Until this is achieved, observations of ice-sheet mass imbalance remain essential in determining their contribution to sea level.

Satellite geodesy has revolutionized the manner in which ice-sheet mass balance is estimated (14, 15). Since 1998, there have been at least 29 ice-sheet mass balance estimates, based variously on the satellite techniques of altimetry, interferometry, and gravimetry (16). These estimates, and their respective uncertainties, allow for a combined Greenland and Antarctic ice-sheet mass im-

balance of between –676 and +69 gigatonnes (Gt) year⁻¹, equivalent to a mean global sea-level contribution in the range of +1.9 to –0.2 mm year⁻¹. However, much of this spread, which is large in comparison to other ice-sheet imbalance assessments (1, 2) and to the estimated rate of global sea-level rise (17), is due to the brevity of many satellite surveys (4.5 years, on average) relative to the rate at which ice-sheet mass fluctuates (5, 18–20). Because the various satellite methods differ in their strengths and weaknesses (14, 15, 21), careful consideration ought to make them complementary. Here, we compare and combine estimates of ice-sheet mass balance derived from all three satellite geodetic techniques, using common spatial and temporal domains, to investigate the extent to which the approaches concur and to produce a reconciled estimate of ice-sheet mass balance.

Data and Methods

In this assessment, we use 19 years of satellite radar altimeter (RA) data, 5 years of satellite laser altimeter (LA) data, 19 years of satellite radar interferometer data, 8 years of satellite gravimetry data, 32 years of surface mass balance (SMB) model simulations, and estimates from several glacial isostatic adjustment models, to produce a reconciled estimate of ice-sheet mass balance. The satellite data sets were developed by using independent methods and, in the case of the LA, gravimeter, and SMB data sets, through contributions from numerous research groups. To enable a direct comparison, we reprocessed the geodetic data sets with use of common time intervals and common definitions of the East Antarctic, West Antarctic, Antarctic Peninsula, and Greenland ice-sheet (EAIS, WAIS, APIS, and GrIS, respectively) boundaries (16). The maximum temporal extent of the satellite data sets spans the period 1992 to 2011, and results from all geodetic techniques are available between January 2003 and December 2008. Unless stated otherwise, all results are presented with 1-sigma uncertainty estimates.

Ice-sheet surface mass balance. SMB includes solid and liquid precipitation, surface sublimation, drifting snow transport, erosion and sublimation, and meltwater formation, refreezing, retention, and runoff. Our estimates of the Antarctic Ice Sheet (AIS) and the GrIS SMB are derived from reconstructions of the RACMO2 regional atmospheric climate model (22) over the period 1979 to 2010, with horizontal resolutions of 27 (AIS) and 11 (GrIS) km. RACMO2 has a multilayer snowpack with drifting snow and snow albedo schemes (23) and has been evaluated against in situ temperature, wind, and surface-energy balance observations from weather stations (24–26) as well as satellite-derived estimates of melt extent, mass changes, and drifting snow (5, 26, 27). The spatial uncertainty of the RACMO2 mean SMB has been assessed through comparison with 310 (GrIS) and 1850 (AIS) in situ observations (28). However, temporal fluctuations in snow accumulation are poorly resolved in observation-

al data sets, so we assess the temporal uncertainty through comparison with global atmospheric reanalyses (16). We also use RACMO2 to drive a model of AIS firn densification (29) for the purpose of converting satellite LA observations into changes in ice-sheet mass.

Glacial isostatic adjustment (GIA). GIA of the solid Earth is an important contributor to the signals observed by satellite gravimetry and, to a lesser extent, satellite altimetry (30). The GIA must therefore be considered when estimating ice-sheet mass balance with either technique. In Antarctica, the use of GIA models has in practice introduced considerable uncertainty (up to 130 Gt year⁻¹) into ice-sheet mass balance estimates derived from satellite gravimetry (31–33). There are a number of contributory factors to this uncertainty, including the scarcity of constraints on the evolution of the ice sheet since the Last Glacial Maximum (LGM), limited knowledge of Earth mechanical properties, and the scarcity of near-field relative sea-level and vertical crustal motion data with which to evaluate model performance (34, 35).

Here, we consider variants of six GIA models, and we assess their impact on geodetic ice-sheet mass balance estimates. For Greenland, where the signal of GIA is relatively small and well constrained, we use the Simpson (36), ICE-5G (37), and ANU (38) models. For Antarctica, we compare the ICE-5G model (39) with two recent Antarctic GIA models: the W12a model (35, 40) and a version (IJ05_R2) of the IJ05 model (41) updated for this study (16). Both regional GIA models incorporate recently improved constraints on the ice-loading history (42–45) that suggest that the AIS was thinner at the LGM than previously thought, leading to a lowering of estimated ice-sheet mass losses since that time (40, 45). Although a consequence of this revision is a potential discrepancy between far-field sea-level records and commonly accepted Northern Hemisphere deglaciation models, both of the new regional GIA models perform well when compared with Antarctic Global Positioning System (GPS) observations (34), and we conclude that these latest solutions are best suited for estimating AIS mass balance.

Radar and laser altimetry. RA and LA provide ice-sheet mass balance estimates through measurements of ice-sheet volume change. The technique has been applied to both Greenland (46–48) and Antarctica (4, 47, 49) and is unique in spatially resolving the detailed pattern of mass imbalance, with monthly temporal sampling. RA provides the longest continuous record of all geodetic techniques (50). Altimeter measurements of elevation change are precise, because they require only modest adjustments to account for sensor drift, changes in the satellite attitude, atmospheric attenuation, and movements of Earth's surface. By far the greatest uncertainty lies in the conversion from volume to mass change. In the case of LA, this conversion has been performed by using an external model of fluctuations in the fir-

¹School of Earth and Environment, University of Leeds, Leeds LS2 9JT, UK. ²Jet Propulsion Laboratory, M/S 300-233, 4800 Oak Grove Drive, Pasadena, CA 91109, USA. ³Department of Physics, University of Colorado, Boulder, CO 80309–0390, USA. ⁴Geodynamics Department, Technical University of Denmark, DTU SPACE, National Space Institute, Elektrovej, Building 327, DK-2800 Kgs. Lyngby, Denmark. ⁵Department of Geography, Durham University, South Road, Durham DH1 3LE, UK. ⁶Center for Space Research, University of Texas at Austin, 3925 West Braker Lane, Suite 200, Austin, TX 78759–5321, USA. ⁷Polar Meteorology Group, Byrd Polar Research Center, and Atmospheric Sciences Program, Department of Geography, The Ohio State University, 1090 Carmack Road, Columbus, OH 43210, USA. ⁸Centre for Polar Observation and Modelling, Department of Earth Sciences, University College London, London WC1E 6BT, UK. ⁹Institut für Astronomische und Physikalische Geodäsie, Technische Universität München, Arcisstraße 21, 80333 München, Germany. ¹⁰Lamont-Doherty Earth Observatory (LDEO), 205 Oceanography, 61 Route 9W - Post Office Box 1000, Palisades, NY 10964, USA. ¹¹Polar Science Center, Applied Physics Laboratory, University of Washington, 1013 NE 40th Street, Seattle, WA 98105–6698, USA. ¹²School of Civil Engineering and Geosciences, Cassie Building, Newcastle University, Newcastle upon Tyne NE1 7RU, UK. ¹³Utrecht University, Institute for Marine and Atmospheric Research, Princetonplein 5, Utrecht, Netherlands. ¹⁴Center for Remote Sensing of Ice Sheets, University of Kansas, Nichols Hall, 2335 Irving Hill Road, Lawrence, KS 66045, USA. ¹⁵Department of Geography, College of Science, Swansea University, Singleton Park, Swansea SA2 8PP, UK. ¹⁶National Aeronautical and Space Administration (NASA) Goddard Space Flight Center, Planetary Geodynamics Laboratory, Greenbelt, MD 20771, USA. ¹⁷Department of Earth Sciences, University of Ottawa, Ottawa, Ontario K1N 6N5, Canada. ¹⁸Department of Earth System Science, University of California, 3226 Croul Hall, Irvine, CA 92697–3100, USA. ¹⁹School of Geographical Sciences, University of Bristol, Bristol BS8 1SS, UK. ²⁰British Antarctic Survey, High Cross, Madingley Road, Cambridge CB3 0ET, UK. ²¹Institute of Meteorology and Geophysics, University of Innsbruck, Innsbruck, Austria. ²²National Snow and Ice Data Center, University of Colorado, Boulder, CO 80309, USA. ²³Delft University of Technology, Faculty of Aerospace Engineering, Kluyverweg 1, 2629 HS Delft, Netherlands. ²⁴SGT Incorporated, NASA Goddard Space Flight Center, Cryospheric Sciences Laboratory, Code 615 Greenbelt, MD 20771, USA. ²⁵Institute for Geophysics, University of Texas, Austin, TX 78759, USA. ²⁶NASA Goddard Space Flight Center, Cryospheric Sciences Laboratory, Code 615 Greenbelt, MD 20771, USA. ²⁷School of Geography and Environmental Studies, University of Tasmania, Hobart 7001, Australia.

*To whom correspondence should be addressed. E-mail: ashepherd@leeds.ac.uk (A.S.); erik.r.ivins@jpl.nasa.gov (E.R.I.)

layer thickness (29, 48, 51). In the case of RA, the conversion to mass has been performed by using a prescribed density model and by allowing for temporal fluctuations in snowfall in the uncertainty (52).

We used European Remote-Sensing (ERS-1 and ERS-2) satellite and Envisat 35-day repeat satellite RA observations to determine changes in the mass of the EAIS and WAIS between May 1992 and September 2010 (16). Time series of surface elevation change were developed at 39,375 crossing points of the satellite orbit ground tracks by using dual-cycle crossovers (49, 53). In total, 46.5 million measurements were included in this analysis, encompassing 74 and 76% of the EAIS and WAIS, respectively. The satellites were cross-calibrated by considering differences between elevation changes occurring during periods of mission overlap. Elevation data were corrected for the lag of the leading-edge tracker and for variations in dry atmospheric mass, water vapor, the ionosphere, solid Earth tides, and surface scattering (50). The IJ05_R2 model was used to correct for elevation changes associated with GIA. Mass changes were calculated by using a surface-density model with a nominal density for firn (400 kg m^{-3}) applied to all regions other than those in which changes are assumed to occur at the density of ice (900 kg m^{-3}) (52). Rates of mass change were computed in regions of interest by interpolating measurements derived at satellite-orbit crossing points and by extrapolating these results to unobserved area. To estimate the uncertainty of mass trends, we treated the estimated variability of snowfall (49) and the elevation trend variability as equivalent sources of uncertainty. This approach is used because it has not yet proved possible to separate, in the observed elevation change, annual cycles due to density fluctuations from residual variations due to signal penetration into the firn.

We used ICESat (Ice, Cloud, and Land Elevation Satellite) LA observations acquired between September 2003 and November 2008 (the period of optimal instrument calibration) to estimate changes in the mass of the AIS and GrIS (16). AIS and GrIS elevation rates were computed by four and two different groups, respectively, using methods that compare surface heights measured along repeated ground tracks. This approach provides fine along-track resolution with high precision (54). However, the ground tracks are widely separated at lower latitudes, and the elevation data are sparsely sampled in time because of the episodic nature of mission campaigns and the presence of clouds. The elevation data were corrected for the effects of GIA by using the W12a model in Antarctica and a combination of models in Greenland, and three groups corrected AIS measurements for estimates of the systematic bias between mission campaigns (32). A variety of approaches were used to isolate observations affected by clouds and to interpolate elevation rates between ground tracks. Elevation rates were adjusted for the effects of short-term

fluctuations in firn thickness by using models driven by either regional climate model predictions (29) or by remotely sensed estimates of temperature (48, 51). The error budget was calculated from uncertainties in the corrected height measurements, in the correction for change in firn thickness, and in the estimated SMB. The mass-change estimates reported here are the arithmetic average of those obtained by the different groups.

Input-output method (IOM). The IOM quantifies the difference between glacier mass gained through snowfall and lost by sublimation and meltwater runoff and the discharge of ice into the ocean. The approach has the advantage of allowing changes in SMB and ice dynamics to be examined separately at the scale of individual glacier drainage basins (5) and has been used in numerous assessments of AIS and GrIS mass balance (18, 55–57). Although earlier IOM studies used representations of SMB developed from guided interpolation of sparse ground observations (58–60), regional atmospheric climate models (5, 61) are now used because they provide sub-daily predictions at high spatial resolution that are independent of the in situ observations. When evaluated against such data, SMB model errors are found to range between 5 and 20%, depending on the basin size and location, with proportionately the largest uncertainties occurring in regions of extreme (low or high) precipitation, strong melting, or where the model resolution is too coarse. Quantifying ice-stream discharge requires measurements of ice velocity and thickness at the grounding line. Ice-sheet velocity snapshots have been widely measured by using interferometric synthetic aperture radar (InSAR) with high (<3%) accuracy (62, 63) and relatively low (annual or longer) frequency. The thickness of many ice streams has been directly measured by using airborne radar with high (~10 m) accuracy (64). Nonetheless, there are many ice-sheet outlet glaciers for which such data do not exist; in these regions, less accurate methods are used to calculate thickness with uncertainties in the range of 80 to 120 m (18, 55). Lastly, where thinning rates are large, the temporal evolution of ice thickness should be accounted for (65).

We used the IOM to determine mass changes of AIS and GrIS drainage basins between January 1992 and June 2010 (16). These results were derived according to the method of (57) and updated to include more recent data sets. SMB estimates for Greenland as reported in (66) were extended to the end of 2010. For Antarctica, the SMB estimates of (61) were used, with an updated uncertainty estimate (28). Ice discharge rates were updated by using new ice-thickness measurements in the Bellingshausen Sea sector, Wilkes Land, and the Amundsen Sea sector; at the grounding line of Filchner Ice Shelf; and at Byrd and Lambert glaciers. Direct measurements of ice thickness are now available for nearly all WAIS ice streams. The IOM inventory, including measured and derived thick-

nesses, now encompasses 64, 79, 96, and 93% of the APIS, EAIS, WAIS, and GrIS, respectively; the remainder is assumed to have no loss due to ice dynamics.

Gravimetry. The Gravity Recovery and Climate Experiment (GRACE) satellite mission has allowed fluctuations in ice-sheet mass to be estimated through measurement of their changing gravitational attraction (32, 67–69). Advantages of the GRACE method are that it provides regional averages without the need for interpolation, measures the effect of mass fluctuations directly, and permits monthly temporal sampling. However, a key challenge is to discriminate fluctuations in ice-sheet mass from changes in the underlying crust and mantle. This is achieved by using models of GIA, which, in the case of the AIS, has led to significant adjustments (70). The spatial resolution of GRACE observations derived from global spherical harmonic solutions of about 300 km in the polar regions (71) is coarse in comparison to that of other geodetic techniques. Hence, a further complicating factor is that signals may leak into regional GRACE solutions as a consequence of remote geophysical processes. In circumstances where spatial relationships between geophysical mass fluxes can be adequately characterized, application of the mass concentration unit (mascon) method (68, 72, 73) introduces a capacity to study changes at smaller scales.

Data from the GRACE satellite mission were used to estimate changes in the mass of the AIS and GrIS between January 2003 and December 2010 (16). Analysis methods varied between the six groups who contributed these observations; some used the mascon approach, whereas others used spatial-averaging kernels. The GRACE data were corrected for the effects of GIA by using the Simpson, ANU, and ICE-5G models in Greenland and the W12a, IJ05_R2, and ICE-5G models in Antarctica. Although we only include results using the W12a and IJ05_R2 models in our reconciled estimates for Antarctica, we also provide separate ice-sheet mass balance estimates determined by using the ICE-5G GIA model solution (16) to allow comparison with previously published estimates; its use leads to more-negative estimates of EAIS mass balance. Each group made its own decisions on processing the GRACE data, including how to combine results by using different GIA models, handle contamination from external sources, compute uncertainties, and compute regional mass trends and time series. Ice-sheet mass time series and trends from all groups were then averaged to obtain the individual GRACE results reported here. For all regions, the mass trends contributed by the individual groups agree with the combined GRACE trend to within the estimated uncertainties.

Results and Discussion

We investigated the extent to which the independent geodetic techniques record similar fluctuations in ice-sheet mass. First, we considered mass

changes within 52 AIS glacier drainage basins as determined by the techniques of satellite RA and IOM (Fig. 1), which are well suited to this task (14, 74). In each case, the 19-year average rate of mass loss from RA was compared with values (55) developed by using the IOM over a similar period. The average difference between the estimates of basin mass imbalance was $1.4 \pm 3.8 \text{ Gt year}^{-1}$, and there is agreement within 1- and 2-sigma uncertainty estimates in 42 and 49 of the 52 basins, respectively. Next, we computed the mass change as determined by satellite RA within areas of the

EAIS and WAIS that were beyond the scope of the IOM survey (55) to assess the extent to which the two methods are complementary (Fig. 1). These two areas, which typically fall between glacier drainage basins of the IOM survey, have small imbalances (4.5 ± 6.0 and $1.4 \pm 1.7 \text{ Gt year}^{-1}$, for the EAIS and WAIS respectively), implying that the region surveyed by the IOM is sufficient to capture the vast majority of the present EAIS and WAIS mass imbalance. Furthermore, the IOM technique is able to resolve important mass changes in regions that are beyond the effective

resolution of the RA survey, such as the APIS (Fig. 1).

As a second example, we investigated the extent to which independent geodetic techniques are able to detect fluctuations in SMB. For this exercise, we considered an exceptional snowfall event in East Antarctica during the first half of 2009 (Fig. 2). A snowfall anomaly that can be identified in CloudSat precipitation data (75) here is clearly apparent within the RACMO2 (and, hence, IOM), RA, and GRACE data sets, which record the firm thickness and mass, volume, and

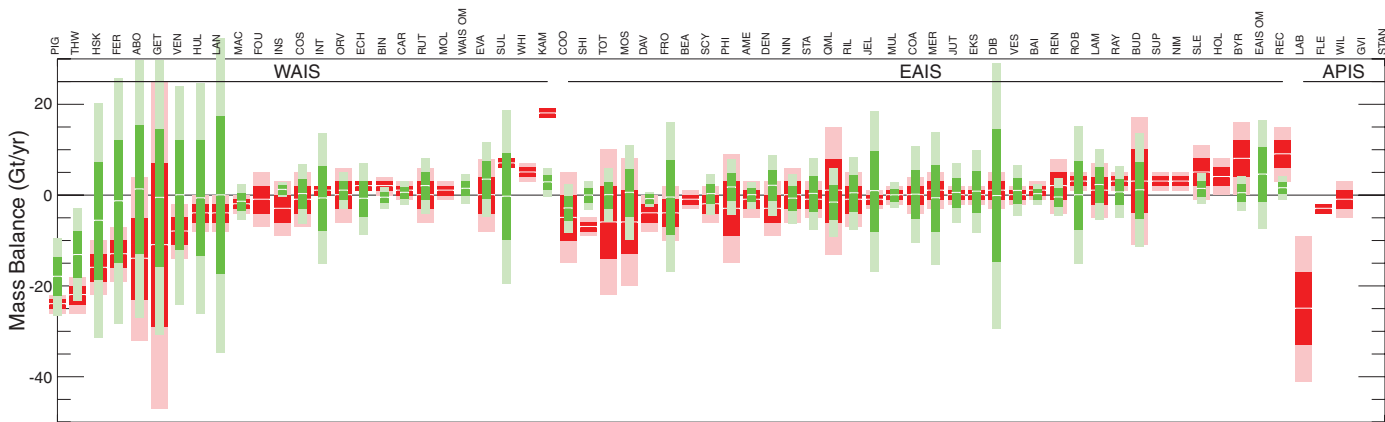


Fig. 1. Comparison of ice sheet mass balance estimates derived from satellite RA (green) and the IOM (red) over the period 1992 to 2011, with 1-sigma and 2-sigma error bars in dark and light shading, respectively, and mean values are shown in white. The comparison is performed for

52 Antarctic drainage basins (55) and the dislocated regions of East and West Antarctica that are omitted from the IOM survey (EAIS_OM and WAIS_OM, respectively). Basin locations are illustrated in the supplementary materials.

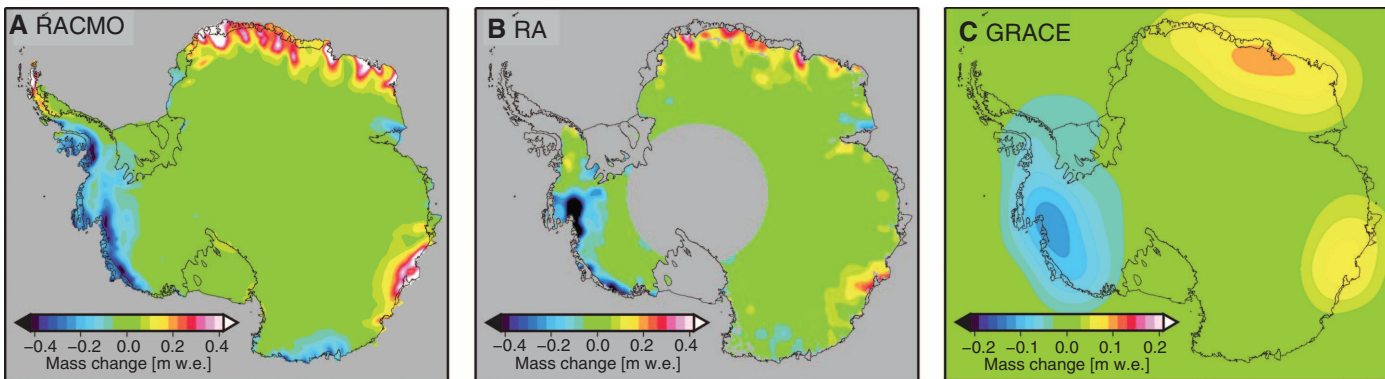
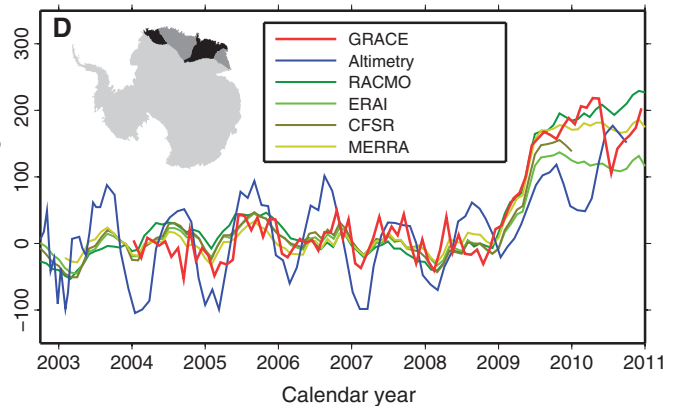


Fig. 2. Estimated anomalies in cumulative ice-sheet firm mass (A), and mass (B and C), derived from the RACMO regional climate model, satellite RA, and GRACE satellite gravimetry, respectively, over a period of anomalously high snowfall in East Antarctica. Anomalies were computed over the period July 2009 to July 2010 relative to July 2008 to July 2009. Before that, linear trends, as fitted to the 2003 to 2008 interval, were removed. The time evolution of the event, as resolved by these data sets and three additional climate models [ERA-Interim (ERA-Interim), CFSR, and MERRA], is also illustrated (D) as the average anomaly over four drainage basins of Dronning Maud Land in East Antarctica (shaded areas in inset map). Although there are SMB fluctuations elsewhere during the same time interval, the pattern of mass loss in West Antarctica is primarily associated with longer-term ice-dynamical imbalance. Relatively large annual cycles are present within some RA time series, but they do not obscure either short- or long-lived events. m w.e., meters water equivalent.



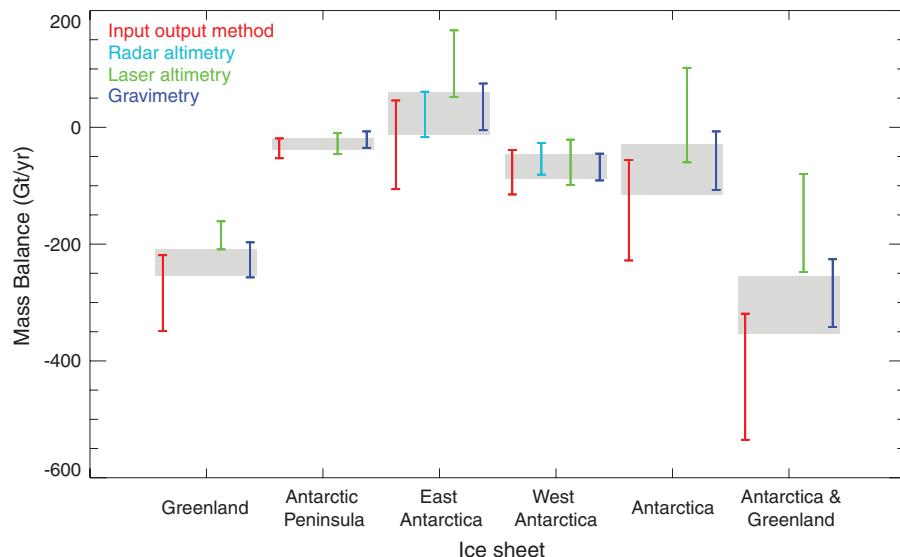


Fig. 3. Intercomparison of mass balance estimates of the GrIS, APIS, EAIS, WAIS, AIS, and the AIS plus GrIS, derived from the four independent geodetic techniques of RA (cyan), IOM (red), LA (green), and gravimetry (blue) over the period 2003 to 2008. Also shown is the reconciled result (gray).

mass fluctuations, respectively. The accumulation event affects the coastal region of the ice sheet, and, although the spatial pattern is best defined by the RACMO2 and altimeter data sets, it is also apparent in the coarser-resolution GRACE data set. Overall, around 200 Gt of additional snow mass was deposited in Dronning Maud Land during this event, equivalent to the mean annual snow accumulation in this sector of Antarctica. In addition to the snowfall anomaly, the RA and GRACE data sets also include ice-dynamical mass changes that fluctuate over the survey period, such as the accelerated mass losses in the Amundsen Sea sector.

In pursuit of a comprehensive methodological intercomparison, we computed changes in the mass of each ice-sheet region between October 2003 and December 2008, the period when all four satellite geodetic techniques were operating optimally (Fig. 3 and table S2). During this 5-year period, which is short relative to the full extent of the geodetic record and in comparison to fluctuations in SMB, the arithmetic means of ice-sheet mass imbalance estimates derived from the available geodetic techniques were -72 ± 43 and -232 ± 23 Gt year⁻¹ for the AIS and the GrIS, respectively. The technique-specific estimates agree with these mean values to within their respective uncertainties in all four ice-sheet regions and for the AIS as a whole. The only exception is the LA estimate of the combined AIS and GrIS mass imbalance, which is, at 140 ± 133 Gt year⁻¹, more positive than the mean value and only marginally beyond the 1-sigma uncertainty range of the respective values. Although the uncertainties of any one particular method are sometimes large, the combination of methods considerably improves the certainty of ice-sheet mass balance estimates.

To produce a reconciled ice-sheet mass balance estimate, we computed the average rate of mass change derived from each of the geodetic techniques within the various regions of interest and over the time periods for which geodetic mass rates were derived (Fig. 4). According to these data, ice-sheet mass balance varies cyclically and by large amounts over intermediate (2- to 4-year) time periods. For example, during the period from 1992 to 2011, the WAIS mass balance fluctuated around a mean value in the range from -50 to -100 Gt year⁻¹, but there have been episodes of considerably larger growth and loss over shorter intervals. Similar variability is apparent in other sectors of the AIS and the GrIS. We next calculated the linear average of the individual estimates of mass balance values to arrive at reconciled values and integrated these data to form a time series of cumulative mass change within each of the four ice-sheet regions (Fig. 5). Although there are obvious dependencies between the mass balance estimates produced by using each of the geodetic techniques, including, for example, the SMB data sets that are common to the IOM and LA processing, the GIA data sets that are common to the gravimetry

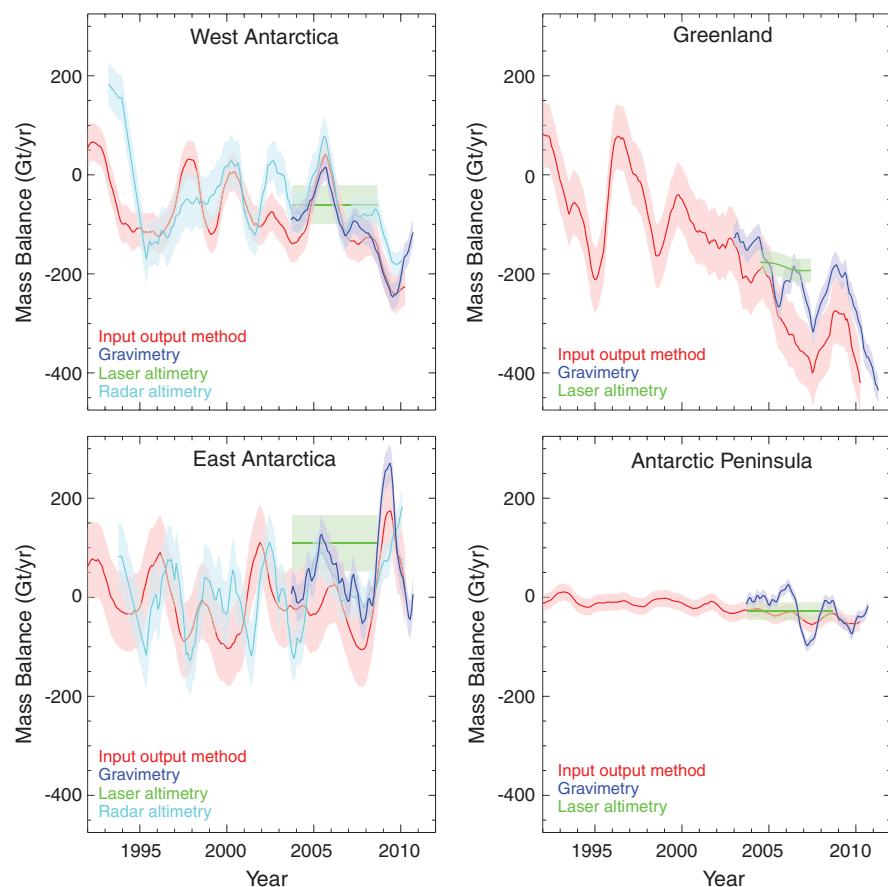


Fig. 4. Rate of mass change of the four main ice-sheet regions, as derived from the four techniques of satellite RA (cyan), IOM (red), LA (green), and gravimetry (blue), with uncertainty ranges (light shading). Rates of mass balance derived from ICESat LA data were computed as constant and time-varying trends in Antarctica and Greenland, respectively. The gravimetry and RA mass trends were computed after applying a 13-month moving average to the relative mass time series. Where temporal variations are resolved, there is often consistency in the interannual variability as determined by the independent data sets.

and altimetry processing, and the orbital corrections that are common to the LA and RA systems, these dependencies are in practice difficult to characterize. For the purpose of calculating the reconciled ice-sheet mass balance estimate, we considered IOM, gravimetry, and altimetry to be independent geodetic techniques. On the basis of this assumption, we compute the standard error of the uncertainty estimates from independent techniques as a measure of their collective uncertainty. Over the course of our 19-year survey, the average rates of mass balance of the AIS and the GrIS were -71 ± 53 and -152 ± 49 Gt year⁻¹, respectively (Table 1). For completeness, we also compute cumulative mass trends by using the data from each individual geodetic technique (fig. S1).

We also computed ice-sheet mass trends over shorter intervals to examine their variability (Table 1). These estimates, along with our integrated time series (Fig. 5), confirm several known signals of mass imbalance, including increasing mass losses from the WAIS (55, 74–77), the APIS (73, 78–80), and the GrIS (5, 81, 82). Although rates of mass loss from the GrIS were modest during the 1990s, they have increased sharply since then because of episodes of glacier acceleration (18, 83) and decreasing SMB (5, 66). GrIS glacier acceleration is, however, neither uniform nor progressive (65, 84, 85), and the large mass losses in 2010 were in fact driven by anomalously low snow accumulation and high runoff (86). The WAIS has lost mass throughout the entire survey period, and our reconciled data set shows

that the rate of mass loss has increased significantly over time (Table 1). The pattern of WAIS imbalance is dominated by mass losses (Amundsen Sea sector) and gains (Kamb Ice Stream) of dynamical origin. Although close to balance during the 1990s, there have been significant mass losses from the APIS since then because of glacier acceleration in the wake of ice-shelf collapse (87, 88) and calving-front retreat (77, 89). The APIS now accounts for around 25% of all mass losses from Antarctic regions that are in a state of negative mass balance, despite occupying just 4% of the continental area. In contrast, the EAIS, which occupies over 75% of Antarctica, was in approximate balance throughout the 1990s. Although the EAIS has experienced mass gains during the final years of our survey (Table 1 and Fig. 5), our reconciled data set is too short to determine whether they were caused by natural fluctuations that are a common feature of Antarctic ice-core records (90) or long-term increases in precipitation that are a common feature of global and regional climate model projections (91–93). Both satellite altimeter data sets highlight the lower reaches of the Cook and Totten Glaciers as regions of ice dynamical mass loss (15, 77), but neither signal is large in comparison with the wider EAIS mass trend. Overall, snowfall-driven mass gains in East Antarctica, notably the anomalous event in Dronning Maud Land during 2009 (Fig. 2), have reduced the rate at which Antarctic ice losses have increased over time, but the EAIS record is too short to determine whether this is a long-term trend.

Our reconciliation exercise has highlighted several other issues. Assessments of GrIS mass balance require more careful consideration than was possible here, because the surrounding mountain glaciers and ice caps are included in some, but not all, of our geodetic surveys and because the ice-sheet domains varied in area by 2%. One estimate has put their contribution at ~ 20 Gt year⁻¹ (94), a value that falls between two we have derived ourselves from ICESat data (10 and 40 Gt year⁻¹). For the EAIS, our mass change estimates exhibit an unsatisfactory spread, with results from the IOM and LA techniques falling consistently lower and higher than the mean value we have derived (table S2). Although the average signal of EAIS imbalance is relatively small, such a large divergence is a matter of concern; improvements of the ancillary data sets that support satellite observations would be of considerable benefit in this region. Lastly, the spatial sampling of mass fluctuations at the APIS is at present inadequate, particularly considering that it provides a significant component of the overall AIS imbalance. Improvements in the spatial and temporal density of satellite observations of this region are needed.

Fig. 5. Cumulative changes in the mass of (left axis) the EAIS, WAIS, and APIS (**top**) and GrIS and AIS and the combined change of the AIS and GrIS (**bottom**), determined from a reconciliation of measurements acquired by satellite RA, the IOM, satellite gravimetry, and satellite LA. Also shown is the equivalent global sea-level contribution (right axis), calculated assuming that 360 Gt of ice corresponds to 1 mm of sea-level rise. Temporal variations in the availability of the various satellite data sets (Fig. 4) means that the reconciled mass balance is weighted toward different techniques during certain periods.

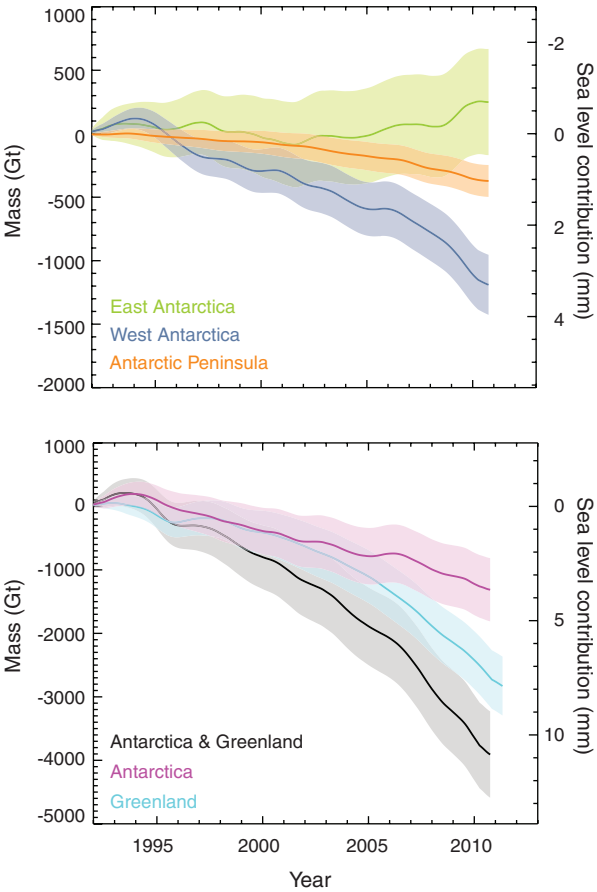


Table 1. Reconciled ice-sheet mass balance estimates determined during various epochs, inclusive of all data present during the given dates. The period 1993 to 2003 was used in an earlier assessment (2).

Region	1992–2011 (Gt/year)	1992–2000 (Gt/year)	1993–2003 (Gt/year)	2000–2011 (Gt/year)	2005–2010 (Gt/year)
GrIS	-142 ± 49	-51 ± 65	-83 ± 63	-211 ± 37	-263 ± 30
APIS	-20 ± 14	-8 ± 17	-12 ± 17	-29 ± 12	-36 ± 10
EAIS	14 ± 43	-2 ± 54	-9 ± 50	26 ± 36	58 ± 31
WAIS	-65 ± 26	-38 ± 32	-49 ± 31	-85 ± 22	-102 ± 18
AIS	-71 ± 53	-48 ± 65	-71 ± 61	-87 ± 43	-81 ± 37
GrIS + AIS	-213 ± 72	-100 ± 92	-153 ± 88	-298 ± 58	-344 ± 48

Conclusions

We estimate that, between 1992 and 2011, the Antarctic and Greenland ice sheets lost 1350 ± 1010 and 2700 ± 930 Gt of ice, respectively, equivalent to an increase in global mean sea level

of 11.2 ± 3.8 mm. The greater certainty and comprehensive nature of this estimate is made possible through our combination of observations derived from a range of geodetic techniques, each of which has different strengths and weaknesses. We have quantified and characterized the ice-sheet imbalance associated with glacier dynamics (the APIS and WAIS), SMB (the EAIS), and a mixture of the two processes (the GrIS). We have also identified the geographical regions where improved data sets are required; the APIS and the EAIS would benefit from measurements with greater spatial sampling and longer temporal sampling, respectively. Although measurements from new and future satellite missions, such as CryoSat-2, may offer new data with which to tackle the former of these challenges, improvements to ancillary data sets are also required. We have shown that assessments of mass imbalance based on short geodetic records should be treated with care, because fluctuations in SMB can be large over short time periods. Lastly, our assessment demonstrates that geodetic assessments of ice-sheet mass balance should consider both the spatial and temporal limitations of the particular data sets upon which they are based and their value in relation to findings based on other independent approaches.

References and Notes

1. J. A. Church, J. M. Gregory, in *Climate Change 2001: The Scientific Basis*, J. T. Houghton et al., Eds. (Cambridge Univ. Press, Cambridge, 2001), pp. 641–693.
2. P. Lemke et al., in *Climate Change 2007: The Physical Science Basis. Contribution of Working Group I to the Fourth Assessment Report of the Intergovernmental Panel on Climate Change*, S. Solomon et al., Eds. (Cambridge Univ. Press, Cambridge, 2007), pp. 337–383.
3. A. J. Payne, A. Vieli, A. P. Shepherd, D. J. Wingham, E. Rignot, *Geophys. Res. Lett.* **31**, L23401 (2004).
4. C. H. Davis, Y. H. Li, J. R. McConnell, M. M. Frey, E. Hanna, *Science* **308**, 1898 (2005).
5. M. van den Broeke et al., *Science* **326**, 984 (2009).
6. R. G. Fairbanks, *Nature* **342**, 637 (1989).
7. J. Turner et al., Eds., *Antarctic Climate Change and the Environment* (Scientific Committee on Antarctic Research, Scott Polar Research Institute, Cambridge, 2009).
8. A. Shepherd et al., *Geophys. Res. Lett.* **37**, L12502 (2010).
9. A. Jenkins et al., *Nat. Geosci.* **3**, 468 (2010).
10. S. S. Jacobs, A. Jenkins, C. F. Giulivi, P. Dutrieux, *Nat. Geosci.* **4**, 519 (2011).
11. A. Shepherd, D. J. Wingham, J. A. D. Mansley, H. F. J. Corr, *Science* **291**, 862 (2001).
12. D. M. Holland, R. H. Thomas, B. de Young, M. H. Ribergaard, B. Lyberth, *Nat. Geosci.* **1**, 659 (2008).
13. G. A. Meehl et al., in *Climate Change 2007: The Physical Science Basis. Contribution of Working Group I to the Fourth Assessment Report of the Intergovernmental Panel on Climate Change*, S. Solomon et al., Eds. (Cambridge Univ. Press, Cambridge, 2007), pp. 747–845.
14. E. Rignot, R. H. Thomas, *Science* **297**, 1502 (2002).
15. A. Shepherd, D. Wingham, *Science* **315**, 1529 (2007).
16. Further information is available at Science Online.
17. N. L. Bindoff et al., in *Climate Change 2007: The Physical Science Basis. Contribution of Working Group I to the Fourth Assessment Report of the Intergovernmental Panel on Climate Change*, S. Solomon et al., Eds. (Cambridge Univ. Press, Cambridge, 2007), pp. 385–432.
18. E. Rignot, P. Kanagaratnam, *Science* **311**, 986 (2006).
19. A. J. Monaghan et al., *Science* **313**, 827 (2006).
20. I. Joughin et al., *Science* **320**, 781 (2008).
21. H. J. Zwally, M. B. Giovinetto, *Surv. Geophys.* **32**, 351 (2011).
22. E. Van Meijgaard et al., “The KNMI regional atmospheric model RACMO version 2.1,” Technical Report 302 (2008).
23. P. K. Munneke et al., *J. Geophys. Res.* **116**, D05114 (2011).
24. J. Ettema et al., *Cryosphere* **4**, 511 (2010).
25. J. H. van Angelen et al., *Cryosphere Discuss.* **6**, 1531 (2012).
26. J. T. M. Lenaerts et al., *J. Geophys. Res.* **117**, D05108 (2012).
27. X. Fettweis, M. Tedesco, M. van den Broeke, J. Ettema, *Cryosphere* **5**, 359 (2011).
28. W. J. van de Berg, thesis, Utrecht University, Utrecht, Netherlands (2008).
29. S. R. M. Ligtenberg, M. M. Helsen, M. R. van den Broeke, *Cryosphere* **5**, 809 (2011).
30. J. Wahr, D. Wingham, C. Bentley, *J. Geophys. Res.* **105**, 16279 (2000).
31. M. Bevis et al., *Geochem. Geophys. Geosyst.* **10**, Q10005 (2009).
32. B. Gunter et al., *J. Geod.* **83**, 1051 (2009).
33. R. E. M. Riva et al., *Earth Planet. Sci. Lett.* **288**, 516 (2009).
34. I. D. Thomas et al., *Geophys. Res. Lett.* **38**, L22302 (2011).
35. P. L. Whitehouse, M. J. Bentley, G. Milne, M. King, I. Thomas, *Geophys. J. Int.* **190**, 1464 (2012).
36. M. J. R. Simpson, G. A. Milne, P. Huybrechts, A. J. Long, *Quat. Sci. Rev.* **28**, 1631 (2009).
37. L. Tarasov, W. R. Peltier, *Geophys. J. Int.* **150**, 198 (2002).
38. K. Fleming, K. Lambeck, *Quat. Sci. Rev.* **23**, 1053 (2004).
39. W. R. Peltier, *Annu. Rev. Earth Planet. Sci.* **32**, 111 (2004).
40. P. L. Whitehouse, M. J. Bentley, A. M. Le Brocq, *Quat. Sci. Rev.* **32**, 1 (2012).
41. E. R. Ivins, T. S. James, *Antarct. Sci.* **17**, 541 (2005).
42. C. Todd, J. Stone, H. Conway, B. Hall, G. Bromley, *Quat. Sci. Rev.* **29**, 1328 (2010).
43. R. P. Ackert Jr. et al., *Earth Planet. Sci. Lett.* **307**, 83 (2011).
44. A. S. Hein, C. J. Fogwill, D. E. Sugden, S. Xu, *Earth Planet. Sci. Lett.* **307**, 211 (2011).
45. A. Mackintosh et al., *Nat. Geosci.* **4**, 195 (2011).
46. O. M. Johannessen, K. Khvorostovsky, M. W. Miles, L. P. Bobylev, *Science* **310**, 1013 (2005).
47. H. J. Zwally et al., *J. Glaciol.* **51**, 509 (2005).
48. H. J. Zwally et al., *J. Glaciol.* **57**, 88 (2011).
49. D. J. Wingham, A. J. Ridout, R. Scharroo, R. J. Arthern, C. K. Shum, *Science* **282**, 456 (1998).
50. D. J. Wingham, D. W. Wallis, A. Shepherd, *Geophys. Res. Lett.* **36**, L17501 (2009).
51. J. Li, H. J. Zwally, *Ann. Glaciol.* **52**, 1 (2011).
52. D. J. Wingham, A. Shepherd, A. Muir, G. J. Marshall, *Philos. Trans. R. Soc. Ser. A* **364**, 1627 (2006).
53. H. J. Zwally, R. A. Bindshadler, A. C. Brenner, J. A. Major, J. G. Marsh, *Science* **246**, 1587 (1989).
54. C. A. Shuman et al., *Geophys. Res. Lett.* **33**, L07501 (2006).
55. E. Rignot et al., *Nat. Geosci.* **1**, 106 (2008).
56. E. Rignot, J. E. Box, E. Burgess, E. Hanna, *Geophys. Res. Lett.* **35**, L20502 (2008).
57. E. Rignot, I. Velicogna, M. R. van den Broeke, A. Monaghan, J. Lenaerts, *Geophys. Res. Lett.* **38**, L05503 (2011).
58. A. Ohmura, N. Reeh, *J. Glaciol.* **37**, 140 (1991).
59. D. G. Vaughan, J. L. Bamber, M. Giovinetto, J. Russell, A. P. R. Cooper, *J. Clim.* **12**, 933 (1999).
60. M. B. Giovinetto, H. J. Zwally, *Ann. Glaciol.* **31**, 171 (2000).
61. J. T. M. Lenaerts, M. R. van den Broeke, W. J. van de Berg, E. van Meijgaard, P. K. Munneke, *Geophys. Res. Lett.* **39**, L04501 (2012).
62. I. Joughin, B. E. Smith, I. M. Howat, T. Scambos, T. Moon, *J. Glaciol.* **56**, 415 (2010).
63. E. Rignot, J. Mougnot, B. Scheuchl, *Science* **333**, 1427 (2011).
64. S. Gogineni et al., *J. Geophys. Res.* **106**, 33761 (2001).
65. I. M. Howat, I. Joughin, T. A. Scambos, *Science* **315**, 1559 (2007).
66. J. Ettema et al., *Geophys. Res. Lett.* **36**, L12501 (2009).
67. I. Velicogna, J. Wahr, *Geophys. Res. Lett.* **32**, L18505 (2005).
68. S. B. Luthcke et al., *Science* **314**, 1286 (2006).
69. J. L. Chen, C. R. Wilson, B. D. Tapley, *J. Geophys. Res.* **116**, B07406 (2011).
70. I. Velicogna, *Geophys. Res. Lett.* **36**, L19503 (2009).
71. B. D. Tapley, S. Bettadpur, J. C. Ries, P. F. Thompson, M. M. Watkins, *Science* **305**, 503 (2004).
72. S. B. Luthcke, A. A. Arendt, D. D. Rowlands, J. J. McCarthy, C. F. Larsen, *J. Glaciol.* **54**, 767 (2008).
73. E. R. Ivins et al., *J. Geophys. Res.* **116**, B02403 (2011).
74. A. Shepherd, D. J. Wingham, J. A. D. Mansley, *Geophys. Res. Lett.* **29**, 1364 (2002).
75. C. Boening, M. Lebosck, F. Landerer, G. Stephens, *Geophys. Res. Lett.* **39**, L21501 (2012).
76. I. Velicogna, J. Wahr, *Nature* **443**, 329 (2006).
77. H. D. Pritchard, R. J. Arthern, D. G. Vaughan, L. A. Edwards, *Nature* **461**, 971 (2009).
78. E. Rignot et al., *Geophys. Res. Lett.* **31**, L18401 (2004).
79. H. Rott, F. Müller, T. Nagler, D. Floricioiu, *Cryosphere* **5**, 125 (2011).
80. E. Berthier, T. A. Scambos, C. A. Shuman, *Geophys. Res. Lett.* **39**, L13501 (2012).
81. W. Krabill et al., *Geophys. Res. Lett.* **31**, L24402 (2004).
82. I. Velicogna, J. Wahr, *Science* **311**, 1754 (2006).
83. I. Joughin, W. Abdalati, M. Fahnestock, *Nature* **432**, 608 (2004).
84. E. J. O. Schrama, B. Wouters, *J. Geophys. Res.* **116**, B02407 (2011).
85. T. Moon, I. Joughin, B. Smith, I. Howat, *Science* **336**, 576 (2012).
86. M. Tedesco et al., *Environ. Res. Lett.* **6**, 014005 (2011).
87. H. Rott, P. Skvarca, T. Nagler, *Antarct. Sci.* **271**, 788 (1996).
88. H. De Angelis, P. Skvarca, *Science* **299**, 1560 (2003).
89. A. J. Cook, A. J. Fox, D. G. Vaughan, J. G. Ferrigno, *Science* **308**, 541 (2005).
90. I. Goodwin, M. de Angelis, M. Pook, N. W. Young, *J. Geophys. Res.* **108**, 16 (2003).
91. P. Uotila, A. H. Lynch, J. J. Cassano, R. I. Cullather, *J. Geophys. Res.* **112**, D10107 (2007).
92. G. Krinner, O. Magand, I. Simmonds, C. Genton, J. L. Dufresne, *Clim. Dyn.* **28**, 215 (2007).
93. T. J. Bracegirdle, W. M. Connolley, J. Turner, *J. Geophys. Res.* **113**, D03103 (2008).
94. R. Hock, M. de Woul, V. Radic, M. Dyurgerov, *Geophys. Res. Lett.* **36**, L07501 (2009).

Acknowledgments: This Ice Sheet Mass Balance Exercise (IMBIE) was facilitated by the European Space Agency and NASA and by a Phillip Leverhulme Prize awarded to A.S. The work was additionally supported by the European Union Framework Programme 7 ice2sea program (ice2sea publication 125), the Lamont Doherty Earth Observatory, NASA (grants NNX09AE47G and NNX08AD64G), the Netherlands Organization for Scientific Research, the Netherlands Polar Program, the UK Natural Environment Research Council, and the NSF. Antarctic glacier ice thickness data used in the IOM calculations were acquired by NASA IceBridge and the Centro de Estudios Científicos Chile, and additional estimates were provided by J. Bamber and J. Griggs. E. van Meijgaard provided assistance with the RACMO model.

Supplementary Materials

www.sciencemag.org/cgi/content/full/338/6111/1183/DC1
Materials and Methods
Supplementary Text
Figs. S1 to S13
Tables S1 to S11
References (95–173)

30 July 2012; accepted 5 October 2012
10.1126/science.1228102